Hindawi
Complexity
Volume 2020, Article ID 5428548, 11 pages
https://doi.org/10.1155/2020/5428548

Research Article

Dynamical Complexity and Multistability in a Novel Lunar Wake Plasma System

Bo. Yan,[1] Punam K. Prasad,[2] Sayan Mukherjee,[3] Asit Saha,[2] and Santo Banerjee[4,5]

[1]*Department of Information Engineering, Shaoyang University, Shaoyang 422000, China*
[2]*Department of Mathematics, Sikkim Manipal Institute of Technology, Sikkim Manipal University, Majitar, Rangpo, East-Sikkim 737136, India*
[3]*Department of Mathematics, Sivanath Sastri College, Kolkata, India*
[4]*Institute for Mathematical Research, Universiti Putra Malaysia, Serdang, Malaysia*
[5]*Malaysia-Italy Centre of Excellence for Mathematical Science, Universiti Putra Malaysia, Serdang, Malaysia*

Correspondence should be addressed to Santo Banerjee; santoban@gmail.com

Received 1 January 2020; Accepted 1 February 2020; Published 16 March 2020

Guest Editor: Viet-Thanh Pham

Dynamical complexity and multistability of electrostatic waves are investigated in a four-component homogeneous and magnetized lunar wake plasma constituting of beam electrons, heavier ions (alpha particles, He^{++}), protons, and suprathermal electrons. The unperturbed dynamical system of the considered lunar wake plasma supports nonlinear and supernonlinear trajectories which correspond to nonlinear and supernonlinear electrostatic waves. On the contrary, the perturbed dynamical system of lunar wake plasma shows different types of coexisting attractors including periodic, quasiperiodic, and chaotic, investigated by phase plots and Lyapunov exponents. To confirm chaotic and nonchaotic dynamics in the perturbed lunar wake plasma, 0 – 1 chaos test is performed. Furthermore, a weighted recurrence-based entropy is implemented to investigate the dynamical complexity of the system. Numerical results show existence of chaos with variation of complexity in the perturbed dynamics.

1. Introduction

The Moon is nonconducting and has no atmosphere and intrinsic magnetic field, so the solar wind freely interacts with the Moon and forms a wake on the antisunward side of the Moon [1]. The magnetic field of solar wind enters the Moon easily compared with particles of solar wind. The variations in density across the boundary of lunar wake steer the solar wind plasma to replenish the void area by ambipolar diffusion [2, 3]. The presence of ion and electron beams with fluctuating temperature of solar wind plasma produces different kinds of waves. The wind satellite revealed ion beams [2] and different modes of nonlinear waves [4] in the tail region of lunar wake. A lunar orbiter SELENE revealed the existence of electrostatic waves which are generated due to the electrostatic instability driven by energetic solar wind particles in the lunar wake [5].

The particles of astrophysical plasmas such as solar wind plasma were generally found to follow non-Maxwellian distribution containing suprathermal particles with high-energy tails [6]. The kappa distribution appropriately defines the influence of suprathermal particles [7]. Recently, Saini [8] and Devanandhan et al. [9] investigated arbitrary nonlinear wave structures in two-temperature plasmas with suprathermal electrons and found the effect of suprathermal electrons on amplitude of solitons.

Some nonlinear systems can exhibit many solutions with specified parameters and distinct initial conditions [10]. This nonlinear behavior is termed as coexisting attractors or multistability. Multistability behaviors [11, 12] of the physical system act as important feature in the dynamics of nonlinear systems. Experimentally, multistability feature was firstly investigated in a Q-switched gas laser [13]; thereafter, various works [14, 15] were reported in different

complex systems exhibiting multistability features. In this study, we show multistability features of the lunar wake plasma system for the first time.

Recently, a new wave structure called supernonlinear wave was introduced in theoretical [16] and astrophysical plasmas [17]. The nonlinear Alfvén waves and solitons defined in the framework of derivative nonlinear Schrodinger equation [18] are found to support supernonlinear waves. Tamang and Saha [19] reported supernonlinear waves and chaotic motion in a non-Maxwellian plasma. Singh and Lakhina [20] investigated ion-acoustic supersolitons in multicomponent plasma. Streaming charged debris moving in space plasma may cause an external disturbance to the system. These disturbances can disrupt the motion of the system [21, 22]. To the best of our knowledge, the study on dynamical properties of nonlinear electrostatic waves in lunar wake plasma is not reported. So, in this work, we employ the concept of nonlinear dynamics to study dynamical properties nonlinear electrostatic structures in magnetized, collisionless, homogeneous plasma comprising of beam electrons, and heavier ions (alpha particles and He^{++}), protons, and kappa distributed electrons.

The article is organized as follows. In Section 2, model equations for the lunar wake plasma system are considered. In Section 3, dynamics of the perturbed and unperturbed system are studied. It has been noticed that the novel system can produce coexisting attractors under the influence of an external forcing term. Variation of Lyapunov exponents shows the conservative nature of the system. To quantify chaos, Lyapunov exponents do not produce constructive information, since very small oscillations of the Lyapunov spectra are observed. To classify chaotic and nonchaotic regimes, 0 − 1 chaos test [23, 24] is then implemented. The analysis is given in Section 4. A dynamical complexity is also investigated by weighted recurrence entropy [25] in Section 5. Section 6 is the conclusion.

2. Model Equations

A homogeneous four-component magnetized lunar wake plasma constituting of protons (N_{p0}, T_p), electron beams (N_{b0}, T_b), heavier ions, such as alpha particles, He^{++} (N_{i0}, T_i), and suprathermal elections (N_{e0}, T_e), where N_{j0} and T_j denote number densities at equilibrium state and temperature of jth species, where $j = b, e, i$, and p for beam electrons and suprathermal electrons, ions, and positrons, respectively. Here, nonlinear electrostatic waves and drift velocity of beam electron (V_{b0}) are assumed to be propagating along the ambient magnetic field (B_0).

The suprathermal electrons of the lunar wake plasma are assumed to follow the κ-distribution [26]:

$$f_e(v) = \frac{n_{e0}}{\pi^{(1/2)}\theta}\frac{\Gamma(k)}{\sqrt{\kappa}\Gamma(k-(1/2))}\left(1+\frac{v^2}{\kappa\theta^2}\right)^{-(\kappa)}, \quad \kappa > \frac{3}{2}, \tag{1}$$

where κ represents spectral index, $\Gamma(\kappa)$ stands for gamma function, and θ denotes modified electron thermal velocity given by

$$\theta^2 = \left(2-\frac{3}{\kappa}\right)\frac{T_e}{m_e}, \tag{2}$$

where T_e and m_e are electron temperature and mass, respectively. The kappa distribution tends to Maxwellian distribution, for $\kappa \longrightarrow \infty$.

The suprathermal electron number density is given by [26]

$$n_e = \left[1-\frac{\phi}{\kappa-(3/2)}\right]^{-\kappa+(1/2)}. \tag{3}$$

The normalized fluid equations for lunar wake plasma propagating parallel to B_0 are given by

$$\frac{\partial n_j}{\partial t} + \frac{\partial\left(n_j v_j\right)}{\partial x} = 0, \tag{4}$$

$$\frac{\partial v_j}{\partial t} + v_j\frac{\partial v_j}{\partial x} + Z_j\mu_{pj}\frac{\partial\phi}{\partial x} + 3\mu_{pj}\sigma_j\frac{n_j}{\left(n_{j0}\right)^2}\frac{\partial n_j}{\partial x} = 0, \tag{5}$$

$$\frac{\partial^2\phi}{\partial x^2} = n_e + n_b - n_p - Z_i n_i, \tag{6}$$

where $\mu_{pj} = (m_p/m_j)$ is the ratio of mass of proton to mass of jth species, $n_0 = n_{e0} + n_{b0} = n_{p0} + Z_i n_{i0}$ is equilibrium number density, and Z_j denotes the electronic charge of the jth species with $Z_p = 1$, $Z_b = -1$, and $Z_i = 2$. In equations (3)–(6), velocity (v_j) is normalized by $C_a = \sqrt{T_e/m_p}$, time by $\omega_{pp}^{-1} = (1/\sqrt{4\pi n_0 e^2/m_p})$, x by $\lambda_D = \sqrt{T_e/4\pi n_0 e^2}$, ϕ by (T_e/e), and n_j by n_0. Furthermore, for one-dimensional case, we consider the adiabatic index, $\gamma_j = 3$ for all species.

3. Dynamical Systems

3.1. Unperturbed Dynamical System. To analyze the dynamical properties of electrostatic waves in lunar wake plasma, we take transformation $\xi = x - Vt$, where V signifies wave speed. Employing ξ and imposing the conditions $\phi \longrightarrow 0$ and $(d\phi/d\xi) = 0$ as $\xi \longrightarrow \pm\infty$ in equations (4)–(5), we obtain

$$n_p = \frac{n_{p0}}{2\sqrt{3\sigma_p}}\left\{\left[\left(V+\sqrt{3\sigma_p}\right)^2 - 2\phi\right]^{1/2} - \left[\left(V-\sqrt{3\sigma_p}\right)^2 - 2\phi\right]^{1/2}\right\}, \tag{7}$$

$$n_i = \frac{n_{i0}}{2\sqrt{3\sigma_i}}\left\{\left[\left(\frac{V}{\sqrt{\mu_{pi}}}+\sqrt{3\sigma_i}\right)^2 - 2Z_i\phi\right]^{1/2} - \left[\left(\frac{V}{\sqrt{\mu_{pi}}}-\sqrt{3\sigma_i}\right)^2 - 2Z_i\phi\right]^{1/2}\right\}, \tag{8}$$

$$n_b = \frac{n_{b0}}{2\sqrt{3\sigma_i}}\left\{\left[\left(\frac{V-V_{b0}}{\sqrt{\mu_{pb}}}+\sqrt{3\sigma_b}\right)^2 + 2\phi\right]^{1/2} - \left[\left(\frac{V-V_{b0}}{\sqrt{\mu_{pb}}}-\sqrt{3\sigma_b}\right)^2 + 2\phi\right]^{1/2}\right\}. \tag{9}$$

Again using equations (3), (7), (8), and (9) in equation (6), we obtain

$$\frac{\mathrm{d}^2\phi}{\mathrm{d}\xi^2} = A\phi + B\phi^2 + C\phi^3 + D\phi^4, \tag{10}$$

where

$$A = \frac{2\kappa-1}{2\kappa-3} - \frac{n_{p0}}{2\sqrt{3\sigma_p}}\left[-\frac{1}{\left(V+\sqrt{3\sigma_p}\right)}+\frac{1}{\left(V-\sqrt{3\sigma_p}\right)}\right] - \frac{n_{i0}}{\sqrt{3\sigma_i}}\left[-\frac{2}{\left(\left(V/\sqrt{\mu_{pi}}\right)+\sqrt{3\sigma_i}\right)}+\frac{2}{\left(\left(V/\sqrt{\mu_{pi}}\right)-\sqrt{3\sigma_i}\right)}\right]$$
$$+\frac{n_{b0}}{2\sqrt{3\sigma_b}}\left[\frac{1}{\left(\left((V-V_{b0})/\sqrt{\mu_{pb}}\right)+\sqrt{3\sigma_b}\right)}-\frac{1}{\left(\left((V-V_{b0})/\sqrt{\mu_{pb}}\right)-\sqrt{3\sigma_b}\right)}\right],$$

$$B = \frac{(2\kappa-1)(2\kappa+1)}{2(2\kappa-3)^2} - \frac{n_{p0}}{2\sqrt{3\sigma_p}}\left[-\frac{1}{2\left(V+\sqrt{3\sigma_p}\right)^3}+\frac{1}{2\left(V-\sqrt{3\sigma_p}\right)^3}\right] - \frac{n_{i0}}{\sqrt{3\sigma_i}}\left[-\frac{2}{\left(\left(V/\sqrt{\mu_{pi}}\right)+\sqrt{3\sigma_i}\right)^3}+\frac{2}{\left(\left(V/\sqrt{\mu_{pi}}\right)-\sqrt{3\sigma_i}\right)^3}\right]$$
$$+\frac{n_{b0}}{2\sqrt{3\sigma_b}}\left[-\frac{1}{2\left(\left((V-V_{b0})/\sqrt{\mu_{pb}}\right)+\sqrt{3\sigma_b}\right)^3}+\frac{1}{2\left(\left((V-V_{b0})/\sqrt{\mu_{pb}}\right)-\sqrt{3\sigma_b}\right)^3}\right],$$

$$C = \frac{(2\kappa-1)(2\kappa+1)(2\kappa+3)}{6(2\kappa-3)^3} - \frac{n_{p0}}{2\sqrt{3\sigma_p}}\left[-\frac{1}{2\left(V+\sqrt{3\sigma_p}\right)^5}+\frac{1}{2\left(V-\sqrt{3\sigma_p}\right)^5}\right] - \frac{n_{i0}}{\sqrt{3\sigma_i}}\left[-\frac{4}{\left(\left(V/\sqrt{\mu_{pi}}\right)+\sqrt{3\sigma_i}\right)^5}+\frac{4}{\left(\left(V/\sqrt{\mu_{pi}}\right)-\sqrt{3\sigma_i}\right)^5}\right]$$
$$+\frac{n_{b0}}{2\sqrt{3\sigma_b}}\left[\frac{1}{2\left(\left((V-V_{b0})/\sqrt{\mu_{pb}}\right)+\sqrt{3\sigma_b}\right)^5}-\frac{1}{2\left(\left((V-V_{b0})/\sqrt{\mu_{pb}}\right)-\sqrt{3\sigma_b}\right)^5}\right],$$

$$D = \frac{(2\kappa-1)(2\kappa+1)(2\kappa+3)(2\kappa+5)}{24(2\kappa-3)^4} - \frac{n_{p0}}{2\sqrt{3\sigma_p}}\left[-\frac{5}{8\left(V+\sqrt{3\sigma_p}\right)^7}+\frac{5}{8\left(V-\sqrt{3\sigma_p}\right)^7}\right] - \frac{n_{i0}}{\sqrt{3\sigma_i}}\left[-\frac{10}{\left(\left(V/\sqrt{\mu_{pi}}\right)+\sqrt{3\sigma_i}\right)^7}+\frac{10}{\left(\left(V/\sqrt{\mu_{pi}}\right)-\sqrt{3\sigma_i}\right)^7}\right]$$
$$+\frac{n_{b0}}{2\sqrt{3\sigma_b}}\left[-\frac{5}{8\left(\left((V-V_{b0})/\sqrt{\mu_{pb}}\right)+\sqrt{3\sigma_b}\right)^7}+\frac{5}{8\left(\left((V-V_{b0})/\sqrt{\mu_{pb}}\right)-\sqrt{3\sigma_b}\right)^7}\right]. \tag{11}$$

Equation (10) is represented as the following dynamical system:

$$\begin{cases} \dfrac{d\phi}{d\xi} = y, \\ \dfrac{dy}{d\xi} = A\phi + B\phi^2 + C\phi^3 + D\phi^4. \end{cases} \tag{12}$$

Here, equation (12) represents a dynamical system with physical parameters κ, n_{b0}, n_{e0}, n_{i0}, n_{p0}, σ_b, σ_i, σ_p, V_{bo}, μ_{pb}, μ_{pi}, and V.

Considering typical parameteric values of lunar wake [3, 26], we set $n_{b0} = 0.01$, $n_{e0} = 0.99$, $n_{i0} = 0.05$, $n_{p0} \approx 0.9$, $\sigma_b = 0.0025$, $\sigma_i = 0.4$, $\sigma_p = 0.2$, and $V_{bo} = 17.14$.

In Figure 1, we present probable phase plots of system (12) for nonlinear electrostatic waves in lunar wake plasma. Based on the values of parameters κ, n_{p0}, n_{i0}, n_{e0}, n_{b0}, σ_p, σ_i, σ_b, V_{bo}, μ_{pb}, μ_{pi}, and V, we have four distinct types of phase plots. Each trajectory in a phase plane corresponds to a traveling wave solution. The phase plots presented in Figure 1 constitute different families of phase trajectories, such as superhomoclinic ($SH_{3,1}$), superperiodic ($SP_{3,1}$), periodic ($P_{1,0}$), and homoclinic ($H_{1,0}$) trajectories which correspond to supersolitary, superperiodic, periodic, and solitary wave solutions of system (12), respectively. Considering different speeds (V) of the nonlinear wave with $\kappa = 5$, $n_{b0} = 0.01$, $n_{e0} = 0.99$, $n_{i0} = 0.05$, $n_{p0} = 0.9$, $\sigma_b = 0.0025$, $\sigma_i = 0.4$, $\sigma_p = 0.2$, $V_{bo} = 17.14$, $\mu_{pb} = 1836$, and $\mu_{pi} = 0.25187$, all qualitatively distinct phase plots are depicted in Figures 1(a)–1(d). If we consider $V = 1.1$ with specified values of other parameters, there exist only two fixed points at $(\phi_0, 0)$ and $(\phi_1, 0)$, as shown in Figure 1(a), where $\phi_0 = 0$ and $\phi_1 < 0$. The two fixed points $(\phi_0, 0)$ and $(\phi_1, 0)$ are the center and saddle point, respectively. The homoclinic trajectory $(H_{1,0})$ at $(\phi_1, 0)$ and a periodic trajectory $(P_{1,0})$ at $(\phi_0, 0)$ correspond to solitary and periodic wave solutions in lunar wake plasma. The phase portrait in Figure 1(b) is presented for $V = 1.225$ with specified values of other parameters. In this case, we obtain a pair of saddle points and centers which occur at $(\phi_0, 0)$, $(\phi_3, 0)$, $(\phi_1, 0)$, and $(\phi_2, 0)$, respectively, where $\phi_1 < 0$ and $\phi_2, \phi_3 > 0$. It shows signatures of superperiodic and supersolitary wave structures due to the presence of $SH_{3,1}$ and $SP_{3,1}$ trajectories. For $V = 1.24$, the existence of four fixed points can still be seen and there exist a pair of $P_{1,0}$ and $H_{1,0}$ trajectories but there is no superperodicity as depicted in Figure 1(c). Figure 1(d) is obtained for $V = 1.3$. In this case, one saddle point at $(\phi_0, 0)$ and a center at $(\phi_1, 0)$ occur, where $\phi_1 < 0$. There also exist a class of $P_{1,0}$ and $H_{1,0}$ trajectories. Thus, the existence of supernonlinear waves (superperiodic and supersoliton) is confirmed in lunar wake for the first time.

3.2. Perturbed Dynamical System. Recently, effect of the Gaussian-shaped source term on nonlinear plasma waves is investigated [27]. But, the nonlinear source term as an external forcing can be of different types [28, 29]. In this work, we consider a source term or perturbation as $f_0 \cos(\omega\xi)$. In presence of the source $f_0 \cos(\omega\xi)$, the dynamical system (12) can be expressed in the following form:

$$\begin{cases} \dfrac{d\phi}{d\xi} = y, \\ \dfrac{dy}{d\xi} = A\phi + B\phi^2 + C\phi^3 + D\phi^4 + f_0 \cos(\omega\xi), \end{cases} \tag{13}$$

where f_0 is the strength and ω is the frequency of the external force.

In Figure 2, we depict possible phase plots of attractors corresponding to system (13) for nonlinear electrostatic structures of lunar wake. We display multistability for different values of ω by varying the initial condition with $\kappa = 5$, $n_{b0} = 0.01$, $n_{e0} = 0.99$, $n_{i0} = 0.05$, $n_{p0} = 0.9$, $\sigma_b = 0.0025$, $\sigma_i = 0.4$, $\sigma_p = 0.2$, $V_{bo} = 17.14$, $\mu_{pb} = 1836$, $\mu_{pi} = 0.25187$, $V = 1.225$, and $f_0 = 0.01$. For $\omega = 0.08$, we obtain Figure 2(a) which shows chaotic and quasiperiodic attractors in ϕy plane with initial conditions $(0, -0.00161)$ (green curve) and $(0, -0.00327)$ (red curve), respectively. In Figure 2(c), we set $\omega = 2.09$ with specified values of other physical parameters and detect the presence of three kinds of attractors which are quasiperiodic, chaotic, and periodic-2 attractors. Quasiperiodic attractors are obtained for initial conditions $(-0.049, 0.0021)$ (blue curve), $(0, 0.011)$ (brown curve), and $(0.049, 0)$ (ocean green curve). Chaotic and periodic-2 attractors are obtained for initial conditions $(-0.049, -0.001897)$ (magenta curve) and $(0.013, 0)$ (black curve), respectively. Here, Figure 2(b) is a part of attractors shown in Figure 2(c). For $\omega = 1.08$, we show chaotic and periodic-1 attractors with initial conditions $(0, -0.0169)$ (red curve) and $(0.21, 0)$ (blue curve), respectively, in Figure 2(d). Thus, multistability behaviors are confirmed in lunar wake plasma in presence of external periodic force.

Lyapunov exponent is an effective tool to check the chaotic motion of any system. For a system to be chaotic, there must be at least one positive Lyapunov exponent. In Figure 3, Lyapunov exponents are plotted against extent of the external periodic force f_0 with specified values of other physical parameters as in Figure 2. Figures 3(a)–3(c) show the Lyapunov exponents corresponding to the chaotic phase trajectories shown in Figures 2(a)–2(d), respectively. From Figure 3, it can be also observed that the fluctuations of Lyapunov exponents are very small (near to 0) in all the cases. So, chaos in (13) cannot be confirmed strongly by the study of the Lyapunov exponent. A test of chaos is thus also performed which is given in the following section.

4. Characterization of Chaos

In this section, we investigate chaos by 0 − 1 test method. In 0 − 1 test method, only one component, say $x(n)_{k=1}^{N}$ (N being the length of the component), of a system is considered [23, 24]. Using the following transformation:

$$\begin{aligned} p(n,c) &= \sum_{j=1}^{n} x(j)\cos(jc), \\ q(n,c) &= \sum_{j=1}^{n} x(j)\sin(jc), \\ & \qquad c \in (0, \pi). \end{aligned} \tag{14}$$

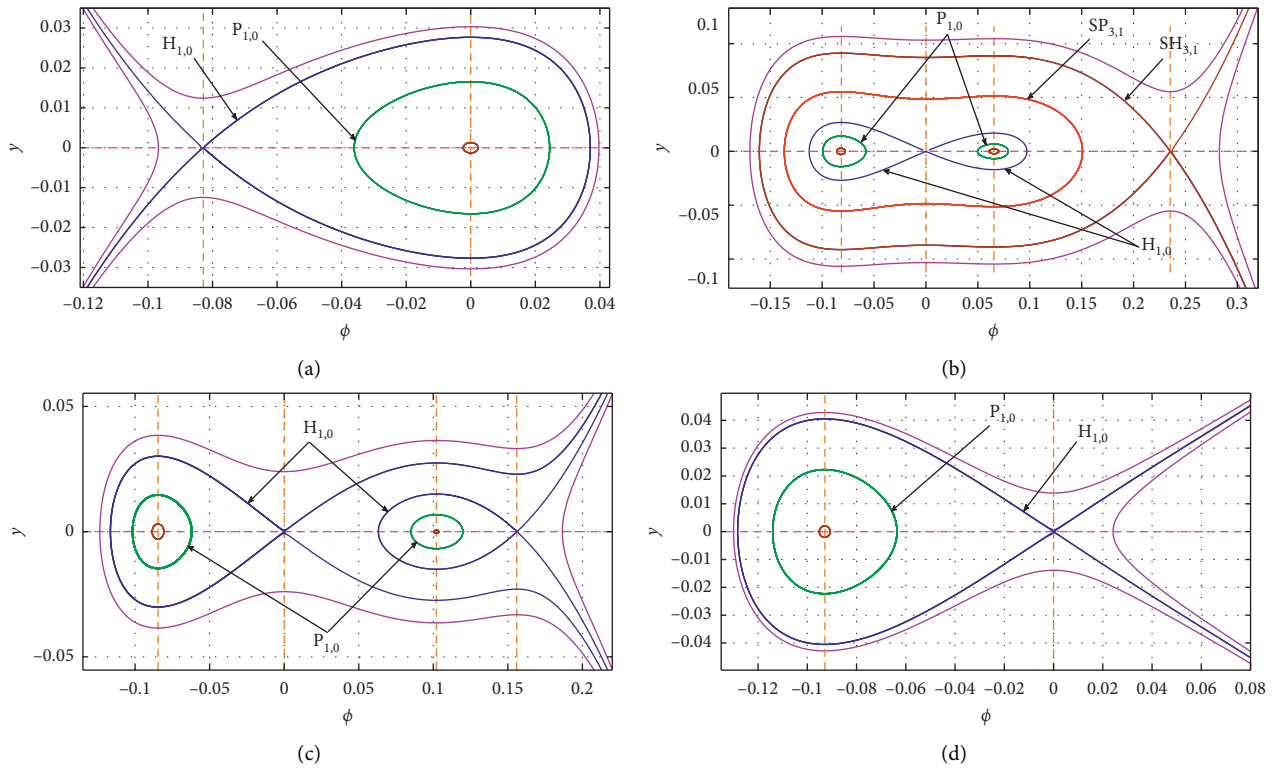

Figure 1: Probable phase plots of the dynamical system (12) for $\kappa = 5$, $n_{b0} = 0.01$, $n_{e0} = 0.99$, $n_{i0} = 0.05$, $n_{p0} = 0.9$, $\sigma_b = 0.0025$, $\sigma_i = 0.4$, $\sigma_p = 0.2$, $V_{bo} = 17.14$, $\mu_{pb} = 1836$, and $\mu_{pi} = 0.25187$ with (a) $V = 1.1$, (b) $V = 1.225$, (c) $V = 1.24$, and (d) $V = 1.3$.

The component $x(n)_{k=1}^{N}$ is decomposed into two components p and q. In [23, 24], it has been established that the chaotic and nonchaotic behavior can be recognized by the respective regular and Brownian motion-like structure in the corresponding (p, q)-plots. So, we investigate nature of the (p, q)-plots for system (13) with the variation of $f_0 \in [0, 0.012]$ and initial conditions $I_k = (0, -k)$, $k \in [0.00161, 0.00327]$. Some of the plots are shown in Figure 4. It can be observed from Figures 4(a) and 4(b) that the corresponding (p, q) clouds are of regular and Brownian motion-like structures, respectively. It indicates nonchaotic and chaotic dynamics in system (13) for the respective $f_0 = 0.001, 0.012$ with $k = 0.00161$. On the contrary, both Figures 4(c) and 4(d) show Brownian-like structure in the corresponding plots with $k = 0.00161, 0.0261$ and $f_0 = 0.012$. Thus, Figure 4 shows chaotic as well as nonchaotic dynamics with the variation of f_0 and k.

In the next, we compute fluctuation of K_c with the variations of $f_0 \in [0, 0.012]$ and $k \in [0.00161, 0.00327]$, where K_c is defined by

$$K_c = \lim_{n \longrightarrow \infty} \frac{\log M_c(n)}{\log n}, \tag{15}$$

where $M_c(n)$ is defined as

$$M_c(n) = \lim_{N \longrightarrow \infty} \frac{1}{N} \sum_{j=1}^{N} \left[p_c(j+n) - p_c(j)\right]^2 + \left[q_c(j+n) - q_c(j)\right]^2. \tag{16}$$

The values of $K_c \approx 0$ and 1 correspond nonchaotic and chaotic dynamics of the system. Figures 5(a) and 5(b) show fluctuation of K_c over $f_0 \in [0, 0.012]$ (fixed $k = 0.0032$) and $k \in [0.00161, 0.00327]$ (fixed $f_0 = 0.012$), respectively. From Figure 5(a), it can be observed that the $K_c \approx 1$ for $f_0 \in [0, 0.0097]$, except $f_0 = 0.004, 0.005, 0.0055$. It assures that chaos in system (13) can only be seen at $f_0 = 0.004, 0.005, 0.0055$ when $f_0 \in [0, 0.0097]$. Furthermore, $K_c \approx 1$ can be seen for $f_0 \in [0.098, 0.12]$. It confirms chaotic dynamics in perturbed system (13) over the region $f_0 \in [0.098, 0.12]$. On the contrary, Figure 5(b) shows $K_c \approx 1$ for almost all values of $k \in [0.00161, 0.00327]$ with fixed $f_0 = 0.012$. It confirms chaos in (13) over $k \in [0.00161, 0.00327]$. We also investigate fluctuation of K_c with the variation of $(f_0, k) \in [0, 0.012] \times [0.00161, 0.00327]$. The corresponding contour is given in Figure 5(c). In Figure 5(c), most of the region shows $K_c \approx 1$, except for few closed regions. It establishes chaotic dynamics of system (13) over $[0, 0.012] \times [0.00161, 0.00327]$, except few values of (f_0, k).

In the following section, we have investigated dynamical complexity using weighted recurrence plot (WRP) [25].

5. Analysis of Dynamical Complexity

For a given n-dimensional phase space $P = \{x_i \in R^n\}$, weighted recurrence $w(i, j)$ is defined by

$$w(i, j) = e^{-\left\|x_i - x_j\right\|}, \quad i, j = 1, 2, \ldots, N, \tag{17}$$

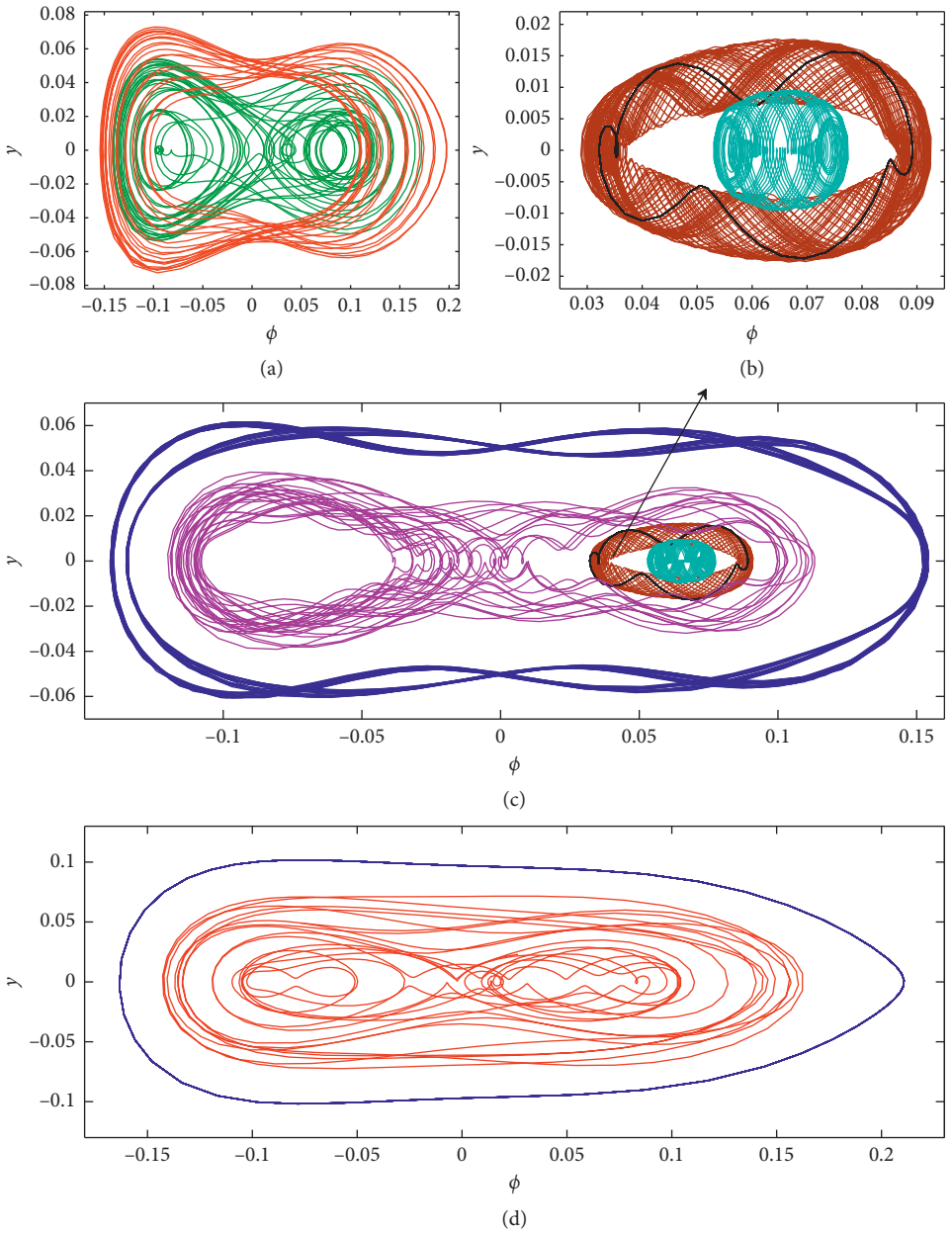

Figure 2: Coexisting attractors of system (13) for $\kappa = 5$, $n_{b0} = 0.01$, $n_{e0} = 0.99$, $n_{i0} = 0.05$, $n_{p0} = 0.9$, $\sigma_b = 0.0025$, $\sigma_i = 0.4$, $\sigma_p = 0.2$, $V_{bo} = 17.14$, $\mu_{pb} = 1836$, $\mu_{pi} = 0.25187$, $V = 1.225$, and $f_0 = 0.01$ and (a) $\omega = 0.08$ with intial conditions $(0, -0.00161)$ (green curve) and $(0, -0.00327)$ (red curve), (b) $\omega = 2.09$ with intial conditions $(0, 0.011)$ (brown curve), $(0.013, 0)$ (black curve), and $(0.049, 0)$ (ocean green curve), (c) enlarged view of coexisting attractors enveloping attractors shown in Figure 2(c) with initial conditions $(-0.049, -0.001897)$ (magenta curve) and $(-0.049, 0.0021)$ (blue curve), and (d) for $\omega = 1.08$ with initial conditions $(0, -0.0169)$ (red curve) and $(0.21, 0)$ (blue curve).

where N is the length of the trajectory of the phase space. As $\|x_i - x_j\|$ indicates dispersion between x_i and x_j, $w(i, j)$ can measure exponential divergence between the trajectories. The corresponding matrix $[w(i, j)]_{N\times N}$ can thus recognize disorder in the phase space. Figures 6(a) and 6(b) represent some of the weighted matrix plots for system (13) with $f_0 = 0.001$ and 0.012 (fixed $k = 0.0032$), respectively. From Figure 6(a), it can be seen that range of variation as well as its pattern in $w(i, j)$ are very less as compared to same in Figure 6(b). It indicates that the corresponding phase space of system (13) at $f_0 = 0.012$ is more complex than the same at $f_0 = 0.001$ for $k = 0.001$. Furthermore, similar investigation is carried out for $k = 0.00161, 0.00261$ with fixed $f_0 = 0.012$. The corresponding weighted matrix plots are shown in Figures 6(c) and 6(d), respectively. As variation in the weights is almost similar between Figures 6(b) and 6(c), same kind of disorder can be observed in the respective phase spaces. On the contrary, completely different as well as various patterns in $[w(i, j)]$ can be seen in Figure 6(d), which indicates higher

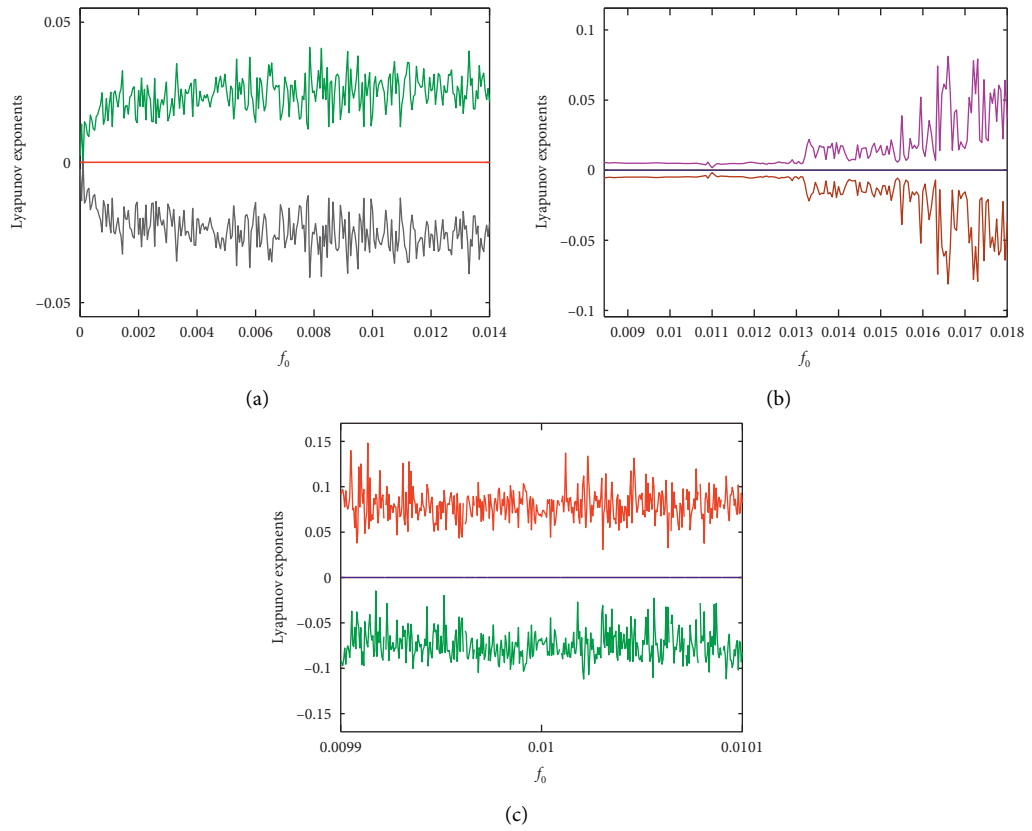

Figure 3: Lyapunov exponents of system (13) of chaotic attractors corresponding to (a) Figure 2(a), (b) Figure 2(c), and (c) Figure 2(d).

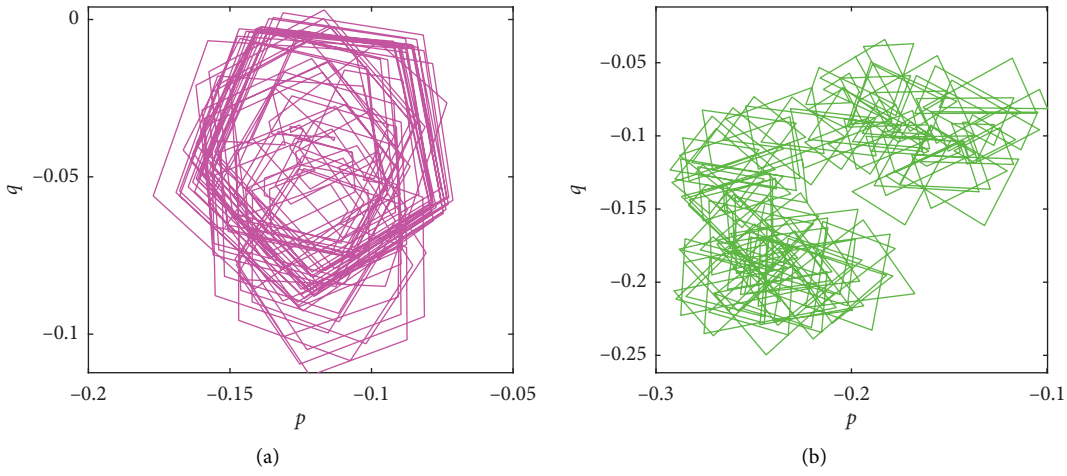

Figure 4: Continued.

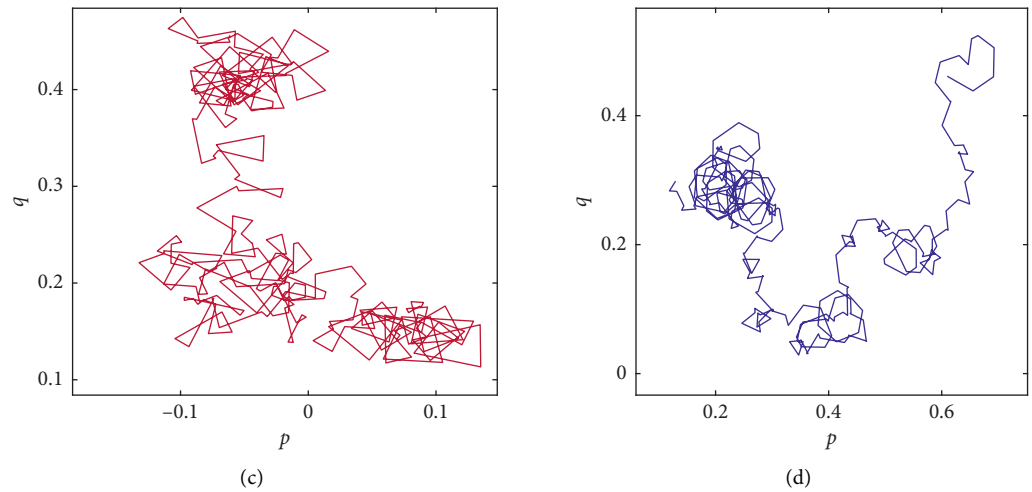

FIGURE 4: (a) and (b) represent (p, q)-plots for system (13) with $f_0 = 0.001$ and 0.012, respectively. In order to calculate p and q, we choose y-component of system (13) with the initial condition $(0, -0.0032)$. Same plots are represented in (c) and (d) with respect to the different initial conditions $(0, -0.00161)$ and $(0, -0.00261)$ for fixed $f_0 = 0.012$. In both the cases, the values of parameters are considered same as chosen in Figure 2. In each calculation, the value of (c) is considered as $(2\pi/3)$.

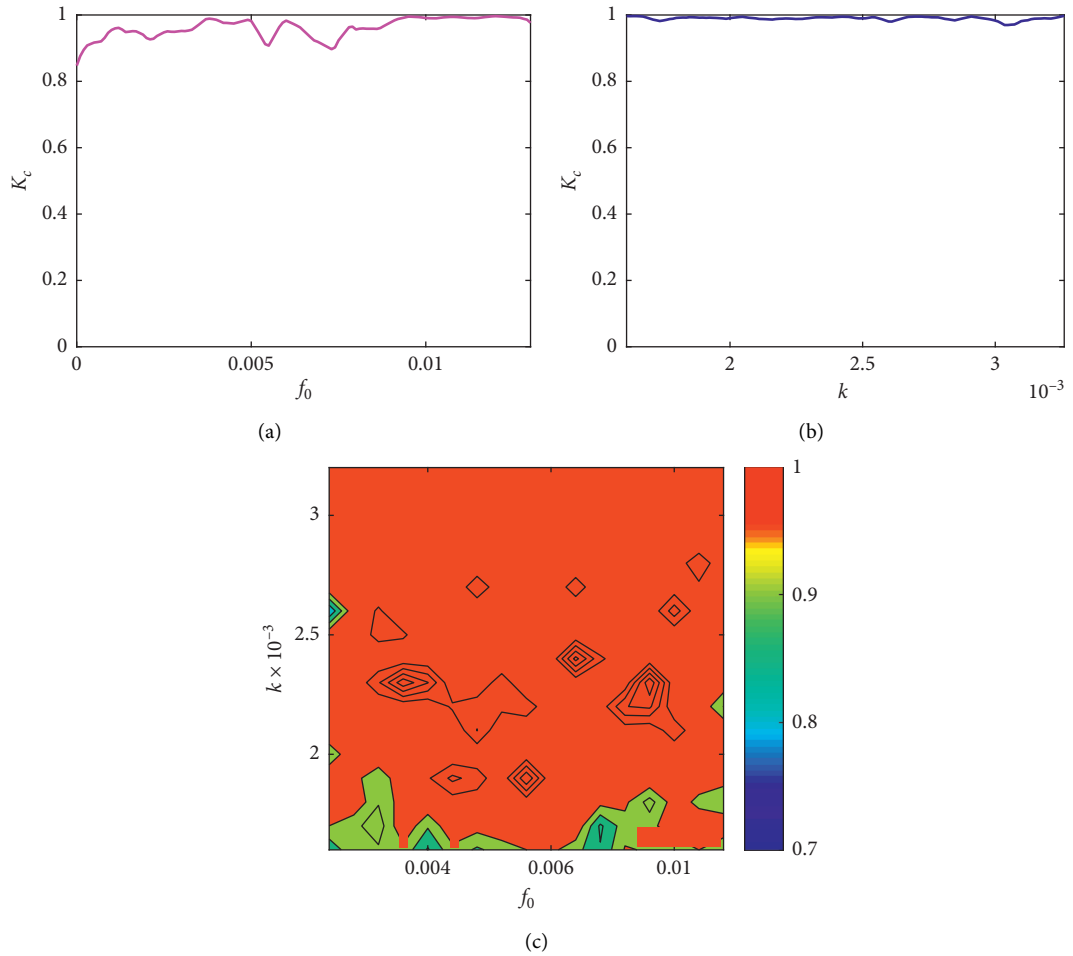

FIGURE 5: (a) represents K_c vs. f_0 graph for system (13) with $f_0 \in [0, 0.013]$ and $k = 0.00161$. (b) represents K_c vs. k for the same system with $k \in [0.00161, 0.00327]$ and $f_0 = 0.012$. (c) represents $[K_c(k, f_0)]$ matrix plot with $k \in [0.00161, 0.00327]$, $f_0 \in [0, 0.013]$. The associated color bar indicates values of K_c over the region $[0.00161, 0.00327] \times [0, 0.013]$. In order to calculate K_c, we have taken $n \ll n_{\text{cut}} = (N/10)$.

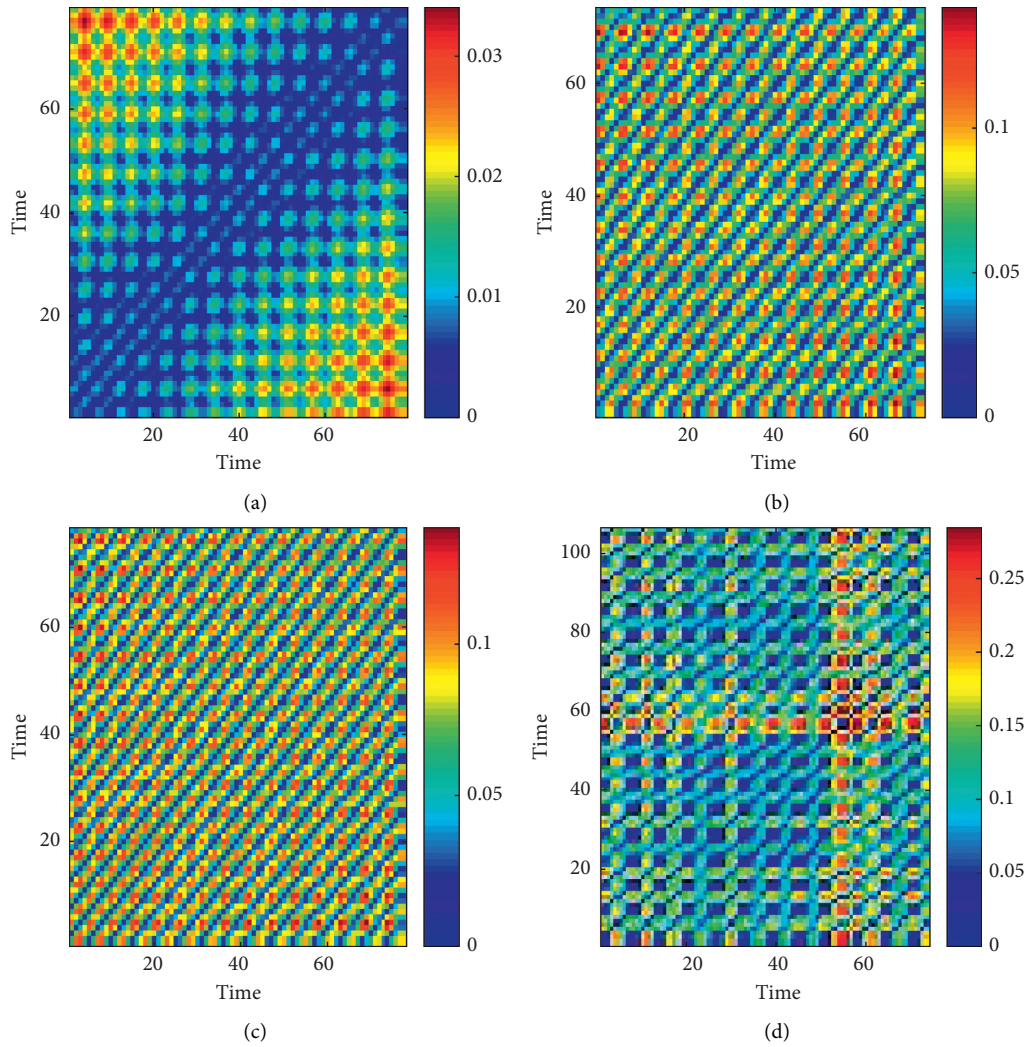

FIGURE 6: (a) and (b) represent $[w(i, j)]$ matrix plots for system (13) with $f_0 = 0.001$ and 0.012, respectively. In order to calculate $[w(i, j)]$ matrix, we solve system (13) with the initial condition $(0, -0.0032)$. Same plots are represented in (c) and (d) with respect to the different initial conditions $(0, -0.00161)$, $(0, -0.00261)$ for fixed $f_0 = 0.012$. In both the cases, the values of parameters are considered same, as chosen in Figure 2. In each calculation, we consider last 10,000 points on the trajectories.

complex structure in the corresponding phase space compared to the other cases.

However, the above mentioned analysis is not enough to understand the complexity for the whole range. This is why we utilize a complexity measure-weighted recurrence entropy measure to investigate how complexity varies with the variations of f_0 and k. The weight recurrence entropy (S_w) is defined as

$$S_w = -\sum_{s_k \in S} p(s_k) \log p(s_k), \tag{18}$$

where $p(s_k)$ denotes probability of $s_k \in S = \{s_k : s_k = (1/N)\sum_{j=1}^{M} \omega_{kj},\ 1 \le k \le M\}$ (M being number of events). In our case, "events" means s_ks.

Using (18), we have computed fluctuation of S_w over $f_0 \in [0, 0.012]$ and $k \in [0.00161, 0.00327]$. Corresponding oscillations are given in Figures 7(a) and 7(b), respectively. An increasing trend can be seen in Figure 7(a). It indicates increasing pattern in the complexity with the increasing $f_0 \in [0, 0.012]$ (fixed $k = 0.0032$). On the contrary, almost parallel trend exists in Figure 7(b). It assures that, variation in S_ws does not fluctuate abruptly. So, complexity does not differ significantly in system (13) with increasing $k \in [-0.00161, -0.00327]$ (fixed $f_0 = 0.012$).

We further investigate complexity of system (13) over the region $(f_0, k) \in [0, 0.012] \times [0.00161, 0.00327]$. The corresponding contour is shown in Figure 7(c). In Figure 7, it can be observed that higher complexity bounded regions are very fewer compared with its complement. However, some discrete increasing as well as decreasing patterns can be seen in the whole contour.

So, the analysis on the novel system reveals that the chaotic dynamics can be observed in system (13) for large regions of f_0 and k, but higher complexity can be seen in the same system for small regions of f_0 and k. Therefore, chaos with high complexity in system (13) for the interval $(f_0, k) \in [0, 0.012] \times [0.00161, 0.00327]$ can be observed.

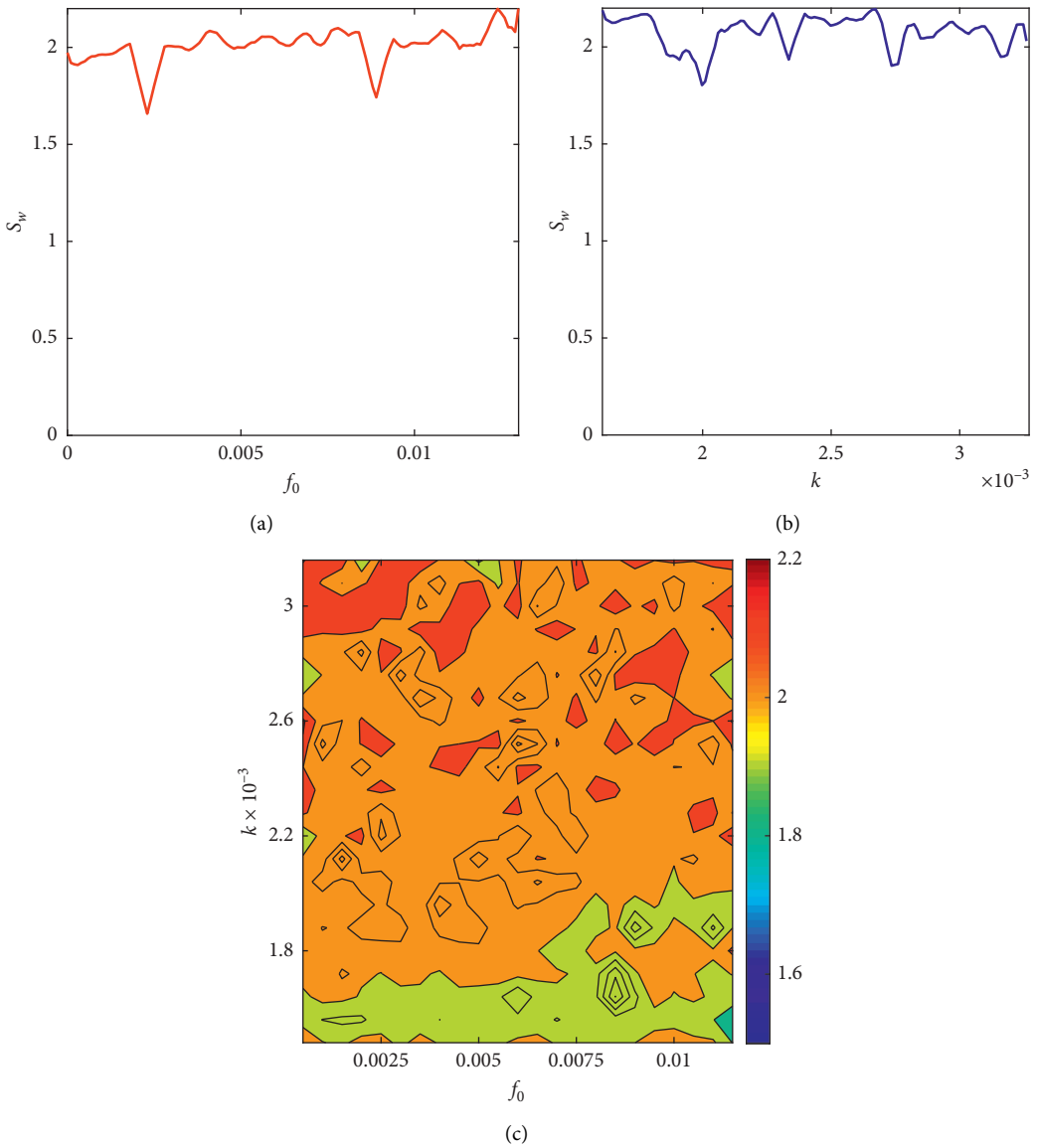

FIGURE 7: (a) and (b) represent $[w(i, j)]$ matrix plots for system (13) with $f_0 = 0.001$ and 0.012, respectively. In order to calculate $[w(i, j)]$ matrix, we solve system (13) with the initial condition $(0, -0.0032)$. Same plots are represented in (c) and (d) with respect to the different initial conditions $(0, -0.00161)$ and $(0, -0.00261)$, for fixed $f_0 = 0.012$. In both the cases, the values of parameters are considered same, as chosen in Figure 2. In each calculation, we consider last 10,000 points on the trajectories.

6. Conclusions

Phase portrait analysis of a novel dynamical system corresponding to lunar wake has been performed in plasma constituting of beam electrons, heavier ions (alpha particles, He^{++}), protons, and suprathermal electrons. Typical values of physical parameters of lunar wake [3, 26] have been applied in the unperturbed system to investigate qualitatively different phase portraits comprising of superperiodic, superhomoclinic, periodic, and homoclinic trajectories. These trajectories correspond to different types of nonlinear and supernonlinear wave solutions. For an external periodic perturbation due to the nonlinear source term, multistability features have been confirmed in a lunar wake plasma system. The existence of multistability in such a plasma model is never been reported. We have also investigated that the system does not confirm chaos with the observations of Lyapunov exponents as the Lyapunov exponents are close to zero with conservative characteristics. To quantify the existence of chaos, we have constructed the $0-1$ test. Furthermore, a detailed dynamical complexity analysis has been implemented by using weighted recurrence. The corresponding results assure that the perturbed system (13) has high complexity in some region inside the parametric space.

Data Availability

No data were used to support this study.

Conflicts of Interest

The authors declare that they have no conflicts of interest.

Acknowledgments

Dr. Asit Saha is grateful to SMIT and SMU for research support funded by TMA Pai University Research Fund-Minor Grant (6100/SMIT/R&D/Project/05/2018).

References

[1] E. Kallio, "Formation of the lunar wake in quasi-neutral hybrid model," *Geophysical Research Letters*, vol. 32, no. 6, p. L06107, 2005.

[2] K. W. Ogilvie, J. T. Steinberg, R. J. Fitzenreiter et al., "Observations of the lunar plasma wake from the WIND spacecraft on December 27, 1994," *Geophysical Research Letters*, vol. 23, no. 10, pp. 1255–1258, 1996.

[3] J. B. Tao, R. E. Ergun, D. L. Newman et al., "Kinetic instabilities in the lunar wake: ARTEMIS observations," *Journal of Geophysical Research: Space Physics*, vol. 117, no. A3, p. A03106, 2012.

[4] P. J. Kellogg, K. Goetz, S. J. Monson, J.-L. Bougeret, R. Manning, and M. L. Kaiser, "Observations of plasma waves during a traversal of the Moon's wake," *Geophysical Research Letters*, vol. 23, no. 10, pp. 1267–1270, 1996.

[5] K. Hashimoto, M. Hashitani, Y. Kasahara et al., "Electrostatic solitary waves associated with magnetic anomalies and wake boundary of the Moon observed by KAGUYA," *Geophysical Research Letters*, vol. 37, no. 19, p. L19204, 2010.

[6] M. M. Selim, A. El-Depsy, and E. F. El-Shamy, "Bifurcations of nonlinear ion-acoustic travelling waves in a multicomponent magnetoplasma with superthermal electrons," *Astrophysics and Space Science*, vol. 360, no. 66, 2015.

[7] V. Pierrard and M. Lazar, "Kappa Distributions: theory and applications in space plasmas," *Solar Physics*, vol. 267, no. 1, p. 153174, 2010.

[8] N. S. Saini, I. Kourakis, and M. A. Hellberg, "Arbitrary amplitude ion-acoustic solitary excitations in the presence of excess superthermal electrons," *Physics of Plasmas*, vol. 16, no. 6, Article ID 062903, 2009.

[9] S. Devanandhan, S. V. Singh, and G. S. Lakhina, "Electron acoustic solitary waves with kappa-distributed electrons," *Physica Scripta*, vol. 84, no. 2, Article ID 025507, 2011.

[10] H. Natiq, M. Said, M. Ariffin, S. He, L. Rondoni, and S. Banerjee, "Self-excited and hidden attractors in a novel chaotic system with complicated multistability," *The European Physical Journal Plus*, vol. 133, no. 12, p. 557, 2018.

[11] H. Natiq, M. R. M. Said, N. M. G. Al-Saidi, and A. Kilicman, "Dynamics and complexity of a new 4d chaotic laser system," *Entropy*, vol. 21, no. 1, p. 34, 2019.

[12] H. Natiq, S. Banerjee, A. P. Misra, and M. R. M. Said, "Degenerating the butterfly attractor in a plasma perturbation model using nonlinear controllers," *Chaos, Solitons & Fractals*, vol. 122, pp. 58–68, 2019.

[13] F. T. Arecchi, R. Meucci, G. Puccioni, and J. Tredicce, "Experimental evidence of subharmonic bifurcations, multistability, and turbulence in aQ-switched gas laser," *Physical Review Letters*, vol. 49, no. 17, pp. 1217–1220, 1982.

[14] H. Natiq, S. Banerjee, S. He, M. Said, and A. Kilicman, "Designing an m-dimensional nonlinear model for producing hyperchaos," *Chaos, Solitons & Fractals*, vol. 114, pp. 506–515, 2018.

[15] H. Natiq, S. Banerjee, M. Ariffin, and M. Said, "Can hyperchaotic maps with high complexity produce multistability?" *Chaos: An Interdisciplinary Journal of Nonlinear Science*, vol. 29, no. 1, Article ID 011103, 2019.

[16] A. E. Dubinov, D. Y. Kolotkov, and M. A. Sazonkin, "Supernonlinear waves in plasma," *Plasma Physics Reports*, vol. 38, no. 10, pp. 833–844, 2012.

[17] A. E. Dubinov and D. Y. Kolotkov, "Above the weak nonlinearity: super-nonlinear waves in astrophysical and laboratory plasmas," *Reviews of Modern Plasma Physics*, vol. 2, no. 1, p. 2, 2018.

[18] T. Hada, C. F. Kennel, and B. Buti, "Stationary nonlinear Alfvén waves and solitons," *Journal of Geophysical Research*, vol. 94, no. A1, p. 65, 1989.

[19] J. Tamang and A. Saha, "Dynamical behavior of supernonlinear positron-acoustic periodic waves and chaos in nonextensive electron-positron-ion plasmas," *Zeitschrift für Naturforschung A*, vol. 74, no. 6, pp. 499–511, 2019.

[20] S. V. Singh and G. S. Lakhina, "Ion-acoustic supersolitons in the presence of non-thermal electrons," *Communications in Nonlinear Science and Numerical Simulation*, vol. 23, no. 1–3, pp. 274–281, 2015.

[21] A. Saha, P. Chatterjee, and C. S. Wong, "Dynamic motions of ion acoustic waves in plasmas with superthermal electrons," *Brazilian Journal of Physics*, vol. 45, no. 6, pp. 656–663, 2015.

[22] L. Mandi, A. Saha, and P. Chatterjee, "Dynamics of ion-acoustic waves in Thomas-Fermi plasmas with source term," *Advances in Space Research*, vol. 64, no. 2, pp. 427–435, 2019.

[23] G. A. Gottwald and I. Melbourne, "A new test for chaos in deterministic systems," *Proceedings of the Royal Society of London. Series A: Mathematical, Physical and Engineering Sciences*, vol. 460, no. 2042, pp. 603–611, 2004.

[24] G. A. Gottwald and I. Melbourne, "Comment on "reliability of the 0-1 test for chaos"," *Physical Review E*, vol. 77, no. 2, Article ID 028201, 2008.

[25] D. Eroglu, T. K. D. M. Peron, N. Marwan et al., "Entropy of weighted recurrence plots," *Physical Review E*, vol. 90, no. 4, Article ID 042919, 2014.

[26] R. Rubia, S. V. Singh, and G. S. Lakhina, "Occurrence of electrostatic solitary waves in the lunar wake," *Journal of Geophysical Research: Space Physics*, vol. 122, no. 9, pp. 9134–9147, 2017.

[27] A. Sen, S. Tiwari, S. Mishra, and P. Kaw, "Nonlinear wave excitations by orbiting charged space debris objects," *Advances in Space Research*, vol. 56, no. 3, pp. 429–435, 2015.

[28] P. Chatterjee, R. Ali, and A. Saha, "Analytical solitary wave solution of the dust ion acoustic waves for the damped forced korteweg-de Vries equation in superthermal plasmas," *Zeitschrift für Naturforschung A*, vol. 73, no. 2, pp. 151–159, 2018.

[29] H. Zhen, B. Tian, H. Zhong, W. Sun, and M. Li, "Dynamics of the Zakharov-Kuznetsov-Burgers equations in dusty plasmas," *Physics of Plasmas*, vol. 20, no. 8, Article ID 082311, 2013.